

Augmented Lagrangian method for a total variation-based model for demodulating phase discontinuities

Journal of Algorithms & Computational Technology
Volume 14: 1–8
© The Author(s) 2020
Article reuse guidelines:
sagepub.com/journals-permissions
DOI: 10.1177/1748302620941413
journals.sagepub.com/home/act



Ricardo Legarda-Saenz  and Carlos Brito-Loeza 

Abstract

In this work, we reformulate the method presented in App. Opt. 53:2297 (2014) as a constrained minimization problem using the augmented Lagrangian method. First we introduce the new method and then describe the numerical solution, which results in a simple algorithm. Numerical experiments with both synthetic and real fringe patterns show the accuracy and simplicity of the resulting algorithm.

Keywords

Phase demodulation, fringe analysis, inverse problems, variational models

Received 4 December 2019; accepted 18 May 2020

Introduction

The main goal of fringe analysis techniques is to recover accurately the local modulated phase from one or several fringe patterns;¹ such phase is related to some physical quantities like shape, deformation, refractive index, temperature, etc. The basic model for a fringe pattern is given by

$$I_{\mathbf{x}} = a_{\mathbf{x}} + b_{\mathbf{x}}\cos(\omega_{\mathbf{x}} + \phi_{\mathbf{x}}) \quad (1)$$

where $\mathbf{x} = (x_1, x_2)$, $a_{\mathbf{x}}$ is the background illumination, $b_{\mathbf{x}}$ is the amplitude modulation, and $\phi_{\mathbf{x}}$ is the phase map to be recovered; the spatial carrier frequency of the fringe pattern is defined by the term $\omega_{\mathbf{x}}$.

Several methods which successfully estimate the phase from a single pattern have been reported in the literature.^{2–5} These methods consider phase maps, amplitude, and illumination terms as a continuous. However, the recovery of a discontinuous phase map from a single fringe pattern remains a pending task and is a challenging problem. Some years ago, a method for computing discontinuous phase maps of a fringe pattern with carrier frequency was proposed, based on the minimization of a regularized cost function, which uses a second-order edge-preserving potential.⁶ Although this method can detect and reconstruct phase discontinuities, its cost functional is not convex, hence

convergence to an optimal solution is conditioned to the provided initial phase usually computed by standard methods.

In recent work, a method for computing discontinuous phase maps based on a total variational (TV) approach was proposed,⁷ where TV regularization is applied to the background, amplitude and phase terms of the fringe model, resulting in accurate phase reconstructions.⁸ Despite this fact, this model lacks a fast algorithm for its solution. Recently, a fixed point (FP) method to speed up the numerical solution of this model was proposed.⁹ This FP method shows a good performance solving the model presented in Legarda-Saenz et al.;⁸ however, similar to other methods based on the TV approach, the FP method performance is dramatically reduced for problems highly anisotropic.

In this work, we reformulate the model presented in Legarda-Saenz et al.⁸ as a constrained minimization problem using augmented Lagrangian method (ALM). First, we describe the ideas that give support

CLIR at Facultad de Matemáticas, Universidad Autónoma de Yucatán, Mérida, México

Corresponding author:

Ricardo Legarda-Saenz, Facultad de Matemáticas, Universidad Autónoma de Yucatán, Apartado Postal 172, Mérida 97110, Yucatán, México.
Email: rlegarda@correo.uady.mx

to our reformulation, and then we describe the numerical solution of the proposed ALM, which results in a simple algorithm. The performance of the proposed method is evaluated by numerical experiments with both synthetic and real data. A comparison against the FP method is presented. Finally we discuss our results and present some concluding remarks.

Methodology

Fixed point method for computing discontinuous phase maps based on TV model

The method proposed for computing discontinuous phase maps based on TV approach⁸ is given by

$$\min_{\phi, a, b} E(\phi_{\mathbf{x}}, a_{\mathbf{x}}, b_{\mathbf{x}}; \omega_{\mathbf{x}}) = \frac{\lambda}{2} \int_{\Omega} (I_{\mathbf{x}} - g_{\mathbf{x}})^2 d\mathbf{x} + \int_{\Omega} |\nabla \phi_{\mathbf{x}}| d\mathbf{x} + \int_{\Omega} |\nabla a_{\mathbf{x}}| d\mathbf{x} + \int_{\Omega} |\nabla b_{\mathbf{x}}| d\mathbf{x} \quad (2)$$

where $\Omega \subset \mathbb{R}^2$ is the domain of integration, $g_{\mathbf{x}}$ is the given fringe pattern, and λ is the regularization parameter. As it was shown in Legarda-Saenz et al.,⁸ this model allows the accurate demodulation of a single fringe pattern with discontinuities. The first-order optimality conditions or Euler–Lagrange equations of equation (2) are given by

$$\begin{aligned} \lambda(I_{\mathbf{x}} - g_{\mathbf{x}}) \frac{\partial I_{\mathbf{x}}}{\partial \phi_{\mathbf{x}}} - \nabla \cdot \frac{\nabla \phi_{\mathbf{x}}}{|\nabla \phi_{\mathbf{x}}|} &= 0, \\ \lambda(I_{\mathbf{x}} - g_{\mathbf{x}}) \frac{\partial I_{\mathbf{x}}}{\partial a_{\mathbf{x}}} - \nabla \cdot \frac{\nabla a_{\mathbf{x}}}{|\nabla a_{\mathbf{x}}|} &= 0, \\ \lambda(I_{\mathbf{x}} - g_{\mathbf{x}}) \frac{\partial I_{\mathbf{x}}}{\partial b_{\mathbf{x}}} - \nabla \cdot \frac{\nabla b_{\mathbf{x}}}{|\nabla b_{\mathbf{x}}|} &= 0 \end{aligned} \quad (3)$$

with boundary conditions

$$\frac{\nabla \phi_{\mathbf{x}}}{|\nabla \phi_{\mathbf{x}}|} \cdot \mathbf{n} = 0, \quad \frac{\nabla a_{\mathbf{x}}}{|\nabla a_{\mathbf{x}}|} \cdot \mathbf{n} = 0, \quad \frac{\nabla b_{\mathbf{x}}}{|\nabla b_{\mathbf{x}}|} \cdot \mathbf{n} = 0 \quad (4)$$

where \mathbf{n} denotes the unit outer normal to the boundary.

The numerical solution proposed in Legarda-Saenz et al.⁸ was a gradient descent scheme which is very slow and therefore a large number of iterations are necessary to reach an adequate solution. To speed up the convergence, a FP method^{10,11} was proposed recently:⁹

First, equation (3) is written in the following way

$$\begin{aligned} \lambda(a_{\mathbf{x}} + b_{\mathbf{x}} \cos \psi_{\mathbf{x}} - g_{\mathbf{x}}) (-b_{\mathbf{x}} \sin \psi_{\mathbf{x}}) - \nabla \cdot \frac{\nabla \phi_{\mathbf{x}}}{|\nabla \phi_{\mathbf{x}}|} &= 0, \\ \lambda(a_{\mathbf{x}} + b_{\mathbf{x}} \cos \psi_{\mathbf{x}} - g_{\mathbf{x}}) (\cos \psi_{\mathbf{x}}) - \nabla \cdot \frac{\nabla b_{\mathbf{x}}}{|\nabla b_{\mathbf{x}}|} &= 0, \\ \lambda(a_{\mathbf{x}} + b_{\mathbf{x}} \cos \psi_{\mathbf{x}} - g_{\mathbf{x}}) - \nabla \cdot \frac{\nabla a_{\mathbf{x}}}{|\nabla a_{\mathbf{x}}|} &= 0 \end{aligned} \quad (5)$$

where the term $\psi_{\mathbf{x}}$ is defined as $\psi_{\mathbf{x}} = \omega_{\mathbf{x}} + \phi_{\mathbf{x}}$.

In Vogel and Oman,¹⁰ a FP method to solve the TV model was proposed. The basic idea is to linearize the nonlinear term of this model, so that at each iteration k the method is required to solve a linear system of the form

$$L_d(d_{\mathbf{x}}^k) d_{\mathbf{x}}^{k+1} = f_d, \quad k = 1, 2, \dots$$

where $d_{\mathbf{x}}$ is the unknown variable, the operator $L_d(\cdot)$ has been made linear by lagging the nonlinear term $\frac{1}{|\nabla a_{\mathbf{x}}|}$, and f_d has the terms which remain constant at each k iteration.

Arranging equation (5) in the same way as described before, the proposed FP iteration is given by

$$\begin{aligned} -\lambda(b_{\mathbf{x}}^k)^2 \sin \psi_{\mathbf{x}}^k \cos \psi_{\mathbf{x}}^{k+1} - \nabla \cdot \frac{\nabla \phi_{\mathbf{x}}^{k+1}}{|\nabla \phi_{\mathbf{x}}^k|} &= \lambda(a_{\mathbf{x}}^k - g_{\mathbf{x}}) (b_{\mathbf{x}}^k \sin \psi_{\mathbf{x}}^k), \\ \left(\lambda \cos^2 \psi_{\mathbf{x}}^k - \nabla \cdot \frac{\nabla}{|\nabla b_{\mathbf{x}}^k|} \right) b_{\mathbf{x}}^{k+1} &= -\lambda(a_{\mathbf{x}}^k - g_{\mathbf{x}}) \cos \psi_{\mathbf{x}}^k, \\ \left(\lambda - \nabla \cdot \frac{\nabla}{|\nabla a_{\mathbf{x}}^k|} \right) a_{\mathbf{x}}^{k+1} &= -\lambda(b_{\mathbf{x}}^k \cos \psi_{\mathbf{x}}^k - g_{\mathbf{x}}) \end{aligned} \quad (6)$$

with $\psi_{\mathbf{x}}^k = \omega_{\mathbf{x}} + \phi_{\mathbf{x}}^k$.

As can be observed in the first term of equation (6), it is not possible to separate the term $\psi_{\mathbf{x}}^{k+1}$ from the cosine function. To fix this, the cosine function is linearized in the following way

$$\cos \psi_{\mathbf{x}}^{k+1} \approx \cos \psi_{\mathbf{x}}^k - (\phi_{\mathbf{x}}^{k+1} - \phi_{\mathbf{x}}^k) \sin \psi_{\mathbf{x}}^k$$

and the proposed FP iteration is given by⁹

$$\begin{aligned} \left(\lambda (b_{\mathbf{x}}^k)^2 \sin^2 \psi_{\mathbf{x}}^k - \nabla \cdot \frac{\nabla}{|\nabla \phi_{\mathbf{x}}^k|} \right) \phi_{\mathbf{x}}^{k+1} &= \lambda (a_{\mathbf{x}}^k b_{\mathbf{x}} \sin \psi_{\mathbf{x}}^k \\ &+ (b_{\mathbf{x}}^k)^2 \cos \psi_{\mathbf{x}}^k \sin \psi_{\mathbf{x}}^k + \phi_{\mathbf{x}}^k (b_{\mathbf{x}}^k)^2 \sin^2 \psi_{\mathbf{x}}^k - g_{\mathbf{x}} b_{\mathbf{x}} \sin \psi_{\mathbf{x}}^k), \\ \left(\lambda \cos^2 \psi_{\mathbf{x}}^k - \nabla \cdot \frac{\nabla}{|\nabla b_{\mathbf{x}}^k|} \right) b_{\mathbf{x}}^{k+1} &= -\lambda (a_{\mathbf{x}}^k \cos \psi_{\mathbf{x}}^k - g_{\mathbf{x}} \cos \psi_{\mathbf{x}}^k), \\ \left(\lambda - \nabla \cdot \frac{\nabla}{|\nabla a_{\mathbf{x}}^k|} \right) a_{\mathbf{x}}^{k+1} &= -\lambda (b_{\mathbf{x}}^k \cos \psi_{\mathbf{x}}^k - g_{\mathbf{x}}) \end{aligned} \quad (7)$$

Brito-Loeza et al.⁹ provide a detailed explanation of the convergence proof and the numerical performance of this method.

Augmented Lagrangian method for TV model

A distinctive feature of the solution proposed in equation (7) is that all the PDE's have the coefficient $1/|\nabla d_{\mathbf{x}}|$, which is quite hard to deal with it numerically due to the inherent discontinuity. A typical solution to this problem is to include a small constant to avoid division by zero, that is $1/\sqrt{|\nabla d_{\mathbf{x}}|^2 + \beta}$, but this affect both the accuracy and efficiency of the solution. Here, we will review an alternative to avoid this problem in a similar TV model. This will prove to be helpful when we introduce our proposed ALM in the next section.

The TV model for image denoising is given by⁷

$$\min_u F_{TV}(u) = \frac{\lambda}{2} \int_{\Omega} (u - f)^2 d\mathbf{x} + \int_{\Omega} |\nabla u| d\mathbf{x} \quad (8)$$

where u is the original image and f is the noisy image. It is well known that the computation of the TV method suffers from non-differentiability due to the TV norm.^{7,12-14} Many numerical methods have been proposed to improve this drawback; one of them is to convert the above functional into a constrained optimization problem, where an auxiliary term is introduced to separate the estimation of the non-differentiable term¹⁵⁻¹⁸

$$\min_{u,q} G_{TV}(u, q) = \frac{\lambda}{2} \int_{\Omega} (u - f)^2 d\mathbf{x} + \int_{\Omega} |q| d\mathbf{x} \quad (9)$$

subject to $q = \nabla u$

where $q = (q_1, q_2)^T$ is the auxiliary term. An efficient solution to the problem shown in equation (9) is using the ALM defined as¹⁸⁻²⁰

$$\min_{u,q} \max_{\mu} L_{TV}(u, q, \mu) = \frac{\lambda}{2} \int_{\Omega} (u - f)^2 d\mathbf{x} + \int_{\Omega} |q| d\mathbf{x} + \int_{\Omega} \mu \cdot (q - \nabla u) d\mathbf{x} + \frac{r}{2} \int_{\Omega} |q - \nabla u|^2 d\mathbf{x} \quad (10)$$

where $\mu = (\mu_1, \mu_2)^T$ is the vector of Lagrange multipliers and r is a positive constant. The iterative process to solve equation (10) is sketched in Algorithm 1.¹⁸⁻²⁰

Algorithm 1: Augmented Lagrangian method for the TV model

Data: $u^0 = 0, q^0 = 0, \mu^0 = 0, k = 0$
while stop criteria is not fulfilled **do**

Solve $(u^{k+1}, q^{k+1}) \approx \min_{u,q} L_{TV}(u, q, \mu^k; f)$ (11)

then update $\mu^{k+1} = \mu^k + r(q^{k+1} - \nabla u^{k+1})$ (12)

$k = k + 1$

end

Equation (11) is an unconstrained optimization problem which is difficult to solve because variables u and q are coupled. One alternative, proposed in literature,^{19,20} is to separate equation (11) in two subproblems defined as

$$\min_u \frac{\lambda}{2} \int_{\Omega} |u - f|^2 d\mathbf{x} - \int_{\Omega} \mu \cdot \nabla u d\mathbf{x} + \frac{r}{2} \int_{\Omega} |q - \nabla u|^2 d\mathbf{x} \quad (13)$$

given the term q , and

$$\min_q \int_{\Omega} |q| d\mathbf{x} + \int_{\Omega} \mu \cdot q d\mathbf{x} + \frac{r}{2} \int_{\Omega} |q - \nabla u|^2 d\mathbf{x} \quad (14)$$

given the term u .

The optimality condition of the problem shown in equation (13) gives a linear equation and can be solved efficiently using the Fourier Transform. On the other side, the problem shown in equation (14) has a closed-form solution known as *soft-thresholding operator*²¹⁻²³ and is defined as^{19,20}

$$q = \begin{cases} \frac{1}{r} \left(1 - \frac{1}{|w|}\right) w, & \text{if } |w| > 1 \\ 0, & \text{if } |w| \leq 1 \end{cases} \quad (15)$$

where $w = r\nabla u - \mu^k$.

Augmented Lagrangian method for computing discontinuous phase maps based on TV model

Following the idea described previously, we transform the problem shown in equation (2) into a constrained one, and then solve it with the ALM. An obvious advantage of using the ALM is that the solution benefits from a fast solver and closed-form solutions. In our case, unfortunately some terms in equation (2) are nonlinear, so a fast solver cannot be used in our solution; however, the described closed-form solutions are susceptible to be used in our approach

The proposed ALM for equation (2) is defined as

$$\begin{aligned}
& \min_{\phi, a, b, \mathbf{q}} \max_{\mu} L(\phi_{\mathbf{x}}, b_{\mathbf{x}}, a_{\mathbf{x}}, \mathbf{q}_{\phi}, \mathbf{q}_b, \mathbf{q}_a, \mu_{\phi}, \mu_b, \mu_a; \omega_{\mathbf{x}}) \\
& = \frac{\lambda}{2} \int_{\Omega} (I_{\mathbf{x}} - g_{\mathbf{x}})^2 d\mathbf{x} + \int_{\Omega} |\mathbf{q}_{\phi}| d\mathbf{x} + \int_{\Omega} |\mathbf{q}_b| d\mathbf{x} + \int_{\Omega} |\mathbf{q}_a| d\mathbf{x} \\
& + \int_{\Omega} \mu_{\phi} \cdot (\mathbf{q}_{\phi} - \nabla \phi_{\mathbf{x}}) d\mathbf{x} + \int_{\Omega} \mu_b \cdot (\mathbf{q}_b - \nabla b_{\mathbf{x}}) d\mathbf{x} \\
& + \int_{\Omega} \mu_a \cdot (\mathbf{q}_a - \nabla a_{\mathbf{x}}) d\mathbf{x} + \frac{r}{2} \int_{\Omega} |\mathbf{q}_{\phi} - \nabla \phi_{\mathbf{x}}|^2 d\mathbf{x} \\
& + \frac{r}{2} \int_{\Omega} |\mathbf{q}_b - \nabla b_{\mathbf{x}}|^2 d\mathbf{x} + \frac{r}{2} \int_{\Omega} |\mathbf{q}_a - \nabla a_{\mathbf{x}}|^2 d\mathbf{x}
\end{aligned} \tag{16}$$

where r is a positive constant, $\mathbf{q}_d = (q_1, q_2)_d^T$ is the auxiliary term, $\mu_d = (\mu_1, \mu_2)_d^T$ are Lagrange multipliers and d is any variable representing ϕ , b , or a .

As can be observed, the functional shown in equation (16) has a similar structure than the one shown in equation (10), so we follow the procedure described in the previous section to propose the solution of equation (16).

The minimization problem given in equation (16) is separated into two subproblems. The first subproblem is related to the solution of the terms $\phi_{\mathbf{x}}$, $b_{\mathbf{x}}$, and $a_{\mathbf{x}}$, given the auxiliary terms \mathbf{q}_{ϕ} , \mathbf{q}_b , and \mathbf{q}_a . This subproblem is defined as

$$\begin{aligned}
& \min_{\phi} \frac{\lambda}{2} \int_{\Omega} (I_{\mathbf{x}} - g_{\mathbf{x}})^2 d\mathbf{x} \\
& \quad - \int_{\Omega} \mu_{\phi} \cdot \nabla \phi_{\mathbf{x}} d\mathbf{x} + \frac{r}{2} \int_{\Omega} |\mathbf{q}_{\phi} - \nabla \phi_{\mathbf{x}}|^2 d\mathbf{x}, \\
& \min_b \frac{\lambda}{2} \int_{\Omega} (I_{\mathbf{x}} - g_{\mathbf{x}})^2 d\mathbf{x} \\
& \quad - \int_{\Omega} \mu_b \cdot \nabla b_{\mathbf{x}} d\mathbf{x} + \frac{r}{2} \int_{\Omega} |\mathbf{q}_b - \nabla b_{\mathbf{x}}|^2 d\mathbf{x}, \\
& \min_a \frac{\lambda}{2} \int_{\Omega} (I_{\mathbf{x}} - g_{\mathbf{x}})^2 d\mathbf{x} \\
& \quad - \int_{\Omega} \mu_a \cdot \nabla a_{\mathbf{x}} d\mathbf{x} + \frac{r}{2} \int_{\Omega} |\mathbf{q}_a - \nabla a_{\mathbf{x}}|^2 d\mathbf{x}
\end{aligned} \tag{17}$$

The second subproblem is related to the solution of the auxiliary terms \mathbf{q}_{ϕ} , \mathbf{q}_b , and \mathbf{q}_a , given the terms $\phi_{\mathbf{x}}$, $b_{\mathbf{x}}$, and $a_{\mathbf{x}}$. This subproblem is defined as

$$\begin{aligned}
& \min_{\mathbf{q}_{\phi}} \int_{\Omega} |\mathbf{q}_{\phi}| d\mathbf{x} + \int_{\Omega} \mu_{\phi} \cdot \mathbf{q}_{\phi} d\mathbf{x} + \frac{r}{2} \int_{\Omega} |\mathbf{q}_{\phi} - \nabla \phi_{\mathbf{x}}|^2 d\mathbf{x}, \\
& \min_{\mathbf{q}_b} \int_{\Omega} |\mathbf{q}_b| d\mathbf{x} + \int_{\Omega} \mu_b \cdot \mathbf{q}_b d\mathbf{x} + \frac{r}{2} \int_{\Omega} |\mathbf{q}_b - \nabla b_{\mathbf{x}}|^2 d\mathbf{x}, \\
& \min_{\mathbf{q}_a} \int_{\Omega} |\mathbf{q}_a| d\mathbf{x} + \int_{\Omega} \mu_a \cdot \mathbf{q}_a d\mathbf{x} + \frac{r}{2} \int_{\Omega} |\mathbf{q}_a - \nabla a_{\mathbf{x}}|^2 d\mathbf{x}
\end{aligned} \tag{18}$$

In the case of the functionals shown in equation (17), the solution can be stated as follows:

The first-order optimality conditions of equation (17) are given by

$$\begin{aligned}
& -\lambda(a_{\mathbf{x}} + b_{\mathbf{x}} \cos \psi_{\mathbf{x}} - g_{\mathbf{x}})(b_{\mathbf{x}} \sin \psi_{\mathbf{x}}) \\
& \quad + \nabla \cdot \mu_{\phi} + r \nabla \cdot (\mathbf{q}_{\phi} - \nabla \phi_{\mathbf{x}}) = 0, \\
& \lambda(a_{\mathbf{x}} + b_{\mathbf{x}} \cos \psi_{\mathbf{x}} - g_{\mathbf{x}})(\cos \psi_{\mathbf{x}}) \\
& \quad + \nabla \cdot \mu_b + r \nabla \cdot (\mathbf{q}_b - \nabla b_{\mathbf{x}}) = 0, \\
& \lambda(a_{\mathbf{x}} + b_{\mathbf{x}} \cos \psi_{\mathbf{x}} - g_{\mathbf{x}}) \\
& \quad + \nabla \cdot \mu_a + r \nabla \cdot (\mathbf{q}_a - \nabla a_{\mathbf{x}}) = 0
\end{aligned} \tag{19}$$

with boundary conditions

$$\begin{aligned}
\mu_{\phi} \cdot \mathbf{n} &= 0, & (\mathbf{q}_{\phi} - \nabla \phi_{\mathbf{x}}) \cdot \mathbf{n} &= 0, \\
\mu_b \cdot \mathbf{n} &= 0, & (\mathbf{q}_b - \nabla b_{\mathbf{x}}) \cdot \mathbf{n} &= 0, \\
\mu_a \cdot \mathbf{n} &= 0, & (\mathbf{q}_a - \nabla a_{\mathbf{x}}) \cdot \mathbf{n} &= 0
\end{aligned}$$

The above equations have the same form than equation (5), so it is possible to express them as the FP iteration shown in equation (7)

$$\begin{aligned}
& (\lambda(b_{\mathbf{x}}^k)^2 \sin^2 \psi_{\mathbf{x}}^k - r \nabla \cdot \nabla) \phi_{\mathbf{x}}^{k+1} = \lambda a_{\mathbf{x}}^k b_{\mathbf{x}}^k \sin \psi_{\mathbf{x}}^k \\
& + \lambda (b_{\mathbf{x}}^k)^2 \cos \psi_{\mathbf{x}}^k \sin \psi_{\mathbf{x}}^k + \lambda \phi_{\mathbf{x}}^k (b_{\mathbf{x}}^k)^2 \sin^2 \psi_{\mathbf{x}}^k \\
& - \lambda g_{\mathbf{x}} b_{\mathbf{x}}^k \sin \psi_{\mathbf{x}}^k - \nabla \cdot \mu_{\phi}^k - r \nabla \cdot \mathbf{q}_{\phi}^k, \\
& (\lambda \cos^2 \psi_{\mathbf{x}}^k - r \nabla \cdot \nabla) b_{\mathbf{x}}^{k+1} = -\lambda (a_{\mathbf{x}}^k \cos \psi_{\mathbf{x}}^k - g_{\mathbf{x}} \cos \psi_{\mathbf{x}}^k) \\
& - \nabla \cdot \mu_b^k - r \nabla \cdot \mathbf{q}_b^k \\
& (\lambda - r \nabla \cdot \nabla) a_{\mathbf{x}}^{k+1} = -\lambda (b_{\mathbf{x}}^k \cos \psi_{\mathbf{x}}^k - g_{\mathbf{x}}) - \nabla \cdot \mu_a^k - r \nabla \cdot \mathbf{q}_a^k
\end{aligned} \tag{20}$$

On the other hand, in the case of the functionals shown in equation (18), we found these to have the same structure that in equation (14), so we can use the *soft-thresholding operator*²¹⁻²³ to solve them

$$\mathbf{q}_d^{k+1} = \begin{cases} \frac{1}{r} \left(1 - \frac{1}{|w_d|}\right) w_d, & \text{if } |w_d| > 1 \\ 0, & \text{if } |w_d| \leq 1 \end{cases} \tag{21}$$

where $w_d = r \nabla a_{\mathbf{x}}^{k+1} - \mu_d^k$, and d is any variable representing ϕ , b , or a .

Finally, the update of the Lagrange multipliers is carried out in the same way it was done in equation (12). The iterative procedure to solve equation (16) is given in Algorithm 2.

Algorithm 2: Augmented Lagrangian method for equation (16)

Data: $\phi_{\mathbf{x}}^0 = 0$, $b_{\mathbf{x}}^0 = 0$, $a_{\mathbf{x}}^0 = 0$, $\mathbf{q}_{\phi}^0 = 0$, $\mathbf{q}_b^0 = 0$, $\mathbf{q}_a^0 = 0$, $\mu_{\phi}^0 = 0$, $\mu_b^0 = 0$, $\mu_a^0 = 0$

$k = 0$

while *stop criteria is not fulfilled* **do**

 Compute ϕ_x^{k+1} , b_x^{k+1} , and a_x^{k+1} using the FP iteration shown in equation (20).

 Compute \mathbf{q}_ϕ^{k+1} , \mathbf{q}_b^{k+1} , and \mathbf{q}_a^{k+1} using equation (21).

 Update

$$\begin{aligned}\mu_\phi^{k+1} &= \mu_\phi^k + r(\mathbf{q}_\phi^{k+1} - \nabla\phi_x^{k+1}) \\ \mu_b^{k+1} &= \mu_b^k + r(\mathbf{q}_b^{k+1} - \nabla b_x^{k+1}) \\ \mu_a^{k+1} &= \mu_a^k + r(\mathbf{q}_a^{k+1} - \nabla a_x^{k+1})\end{aligned}\quad (22)$$

$k = k + 1$

end

Numerical experiments

To illustrate the performance of the ALM, we carried out some numerical experiments using a Intel Core i7 @ 2.40 GHz laptop with Debian GNU/Linux 9 (64-bit) and 16 GB of memory. In these experiments, we compare our proposed method with the FP method shown in equation (7). Both methods were implemented in C/C++. In our experiments, we used as stopping criteria the following condition

$$\frac{\|d^k - d^{k-1}\|}{\|d^{k-1}\|} \leq \epsilon$$

where $\epsilon = 10^{-5}$ and d is any variable representing ϕ , b , or a . For the ALM we use $r = 11.5$, and for the FP method we use $\beta = 10^{-3}$, which is the constant to avoid division by zero.

For simplicity, we selected the regularization parameter λ manually. However, well known methods can be used to obtain the best parameter for this task, such as those described in section 5.6 of Bertero and Boccacci.²⁴ In addition, we use a normalized error Q to compare the phase-map estimation; this error is defined as²⁵

$$Q(\mu, \nu) = \frac{\|\mu - \nu\|_2}{\|\mu\|_2 + \|\nu\|_2}$$

where μ and ν are the signals to be compared. The normalized error values vary between zero (for perfect agreement) and one (for total disagreement).

Phase demodulation using synthetic fringe pattern

Here we present two experiments using a synthetic fringe pattern of size 640×480 pixels, generated in

similar way to that described in literature.^{6,8} Figure 1 shows the synthetic fringe pattern and the synthetic phase term ϕ_x .

The first experiment was the demodulation of this fringe pattern using the ALM and the FP method, both with $\lambda = 10$. The resultant phase demodulations are shown in Figure 2. In Figure 3, we show the middle row of the estimated phase term ϕ_x . The normalized error of the ALM was $Q = 0.0243$ and the time employed to obtain the solution was 141 s using 655 iterations. On the other hand, the normalized error of the FP method was $Q = 0.0343$ and the time employed to obtain the solution was 340 s using 841 iterations.

In Figure 2, it can be seen that both methods successfully demodulate the discontinuity found in the synthetic fringe pattern. However, when analyzing Figure 3, we found that the demodulation of the proposed ALM is more precise than that of the FP method. Moreover, the time and number of iterations employed to obtain the solution are better than the FP method. This is due to the influence of the term β on the performance of the FP method: with a larger value of this term, the speed of convergence of the method is better but the accuracy of the solution gets worse. This is not desirable in fringe analysis techniques.

The second experiment was the demodulation of the fringe pattern shown in Figure 2 with different levels of noise. In this experiment, we used $\lambda = 6$ for both the methods. The resultant performance of both methods is shown in Figure 4. As can be observed, in this experiment we found the same differences mentioned

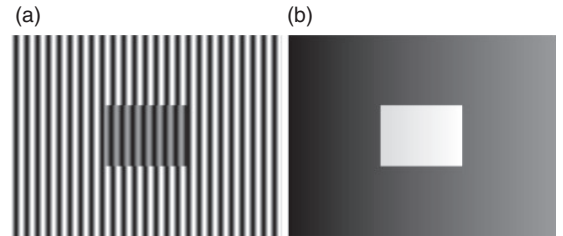


Figure 1. (a) Synthetic fringe pattern. (b) Synthetic phase term ϕ_x .

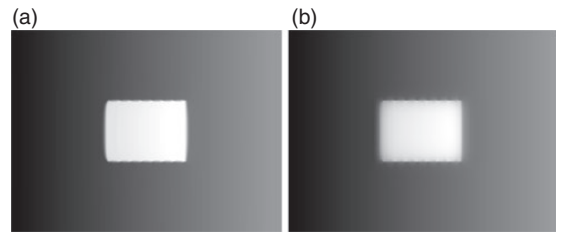


Figure 2. Estimated phase terms using (a) augmented Lagrangian method, equation (16), and (b) fixed point method, equation (7).

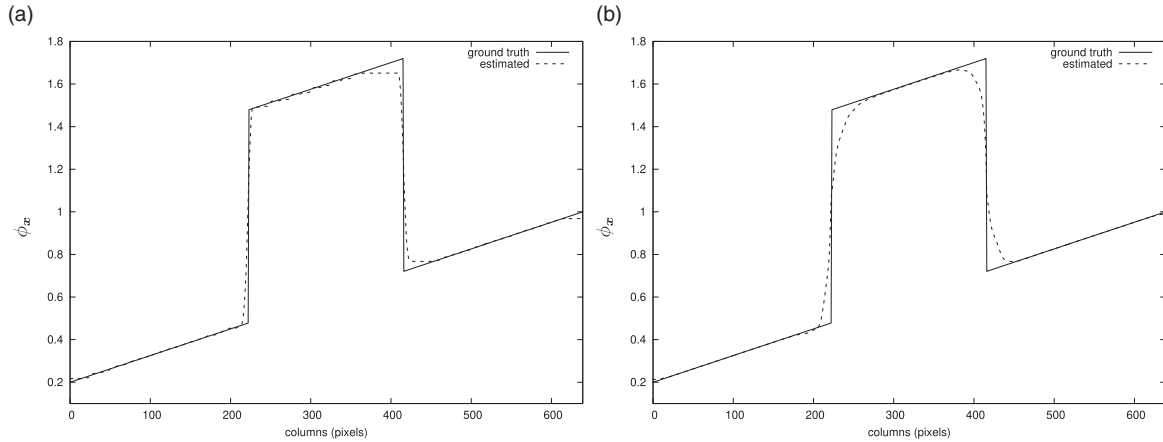


Figure 3. Middle row of the estimated phase terms using (a) augmented Lagrangian method, equation (16), and (b) fixed point method, equation (7).

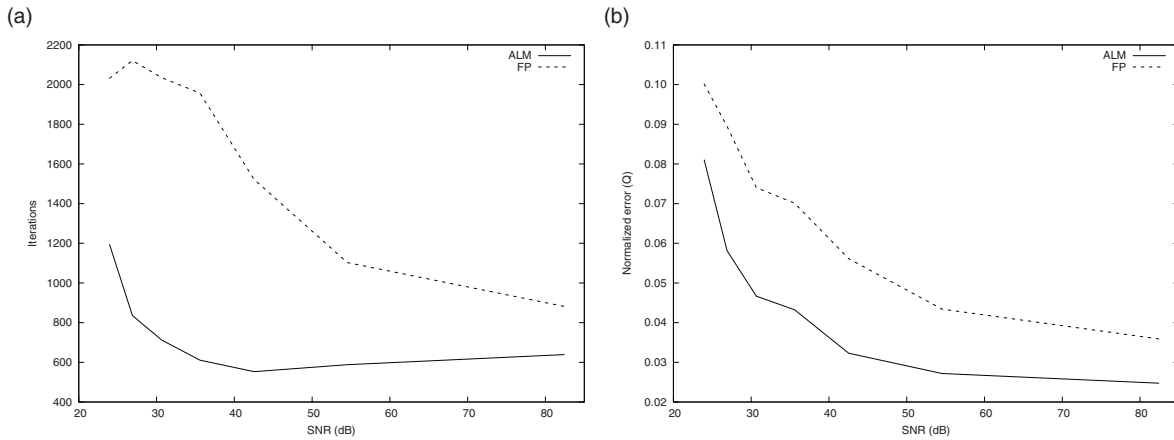


Figure 4. Performance of the phase demodulation methods with different noise levels: (a) iterations employed and (b) the normalized error Q .

previously: the proposed ALM demodulates the fringe pattern faster and more accurately than the FP method, even with noisy fringe patterns.

Phase demodulation using experimental fringe patterns

Here we present the phase demodulation of a fringe pattern obtained from a holographic interferometry experiment,²⁶ which consisted of the height measurement of a micro-thin film. The fringe pattern obtained from this experiment, with 640×480 pixels, is shown in Figure 5(a). Figure 5(b) shows a phase term ϕ_x estimation of this experimental fringe pattern using Schwider–Hariharan (4 + 1) algorithm.^{1,26} This estimation was used as a reference in this experiment.

The demodulations of this experimental fringe pattern using the ALM and the FP method are shown in

Figure 6, both with $\lambda = 10$. In Figure 7, we show the middle column of the estimated phase term ϕ_x . The time employed by the ALM to obtain the solution was 430 s using 1995 iterations. On the other hand, the FP method took 3288 s using 7445 iterations to obtain the solution.

As can be observed in Figures 6 and 7, both methods are able to demodulate the discontinuity found in the experimental fringe pattern. These estimations can be seen as the filtered version of the one shown in Figure 5 (b). One relevant aspect is that both methods preserve the dynamic range of the phase term ϕ_x . On the other hand, there are marked differences in the quality of the estimation and in the numerical performance to obtain it: the proposed ALM delivers a piecewise constant surface while the FP method gives a smoother one. Additionally, our proposal is several times faster than the FP method.

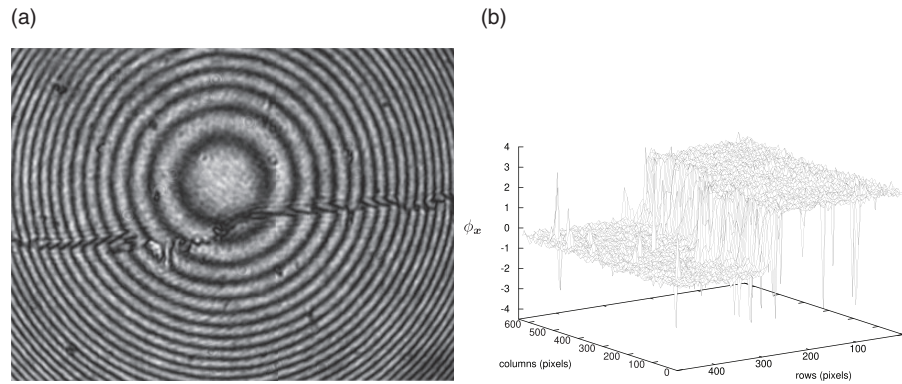


Figure 5. (a) Experimental fringe pattern. (b) Estimated phase term ϕ_x using Schwider–Hariharan (4 + 1) algorithm.^{1,26}

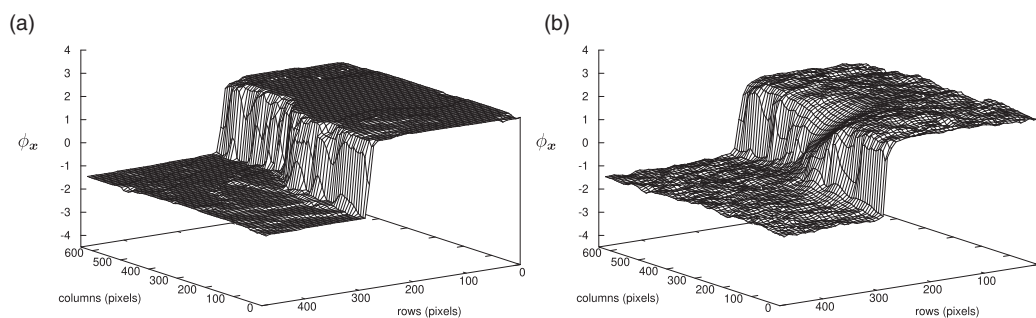


Figure 6. Estimated phase terms using (a) augmented Lagrangian method, equation (16), and (b) fixed point method, equation (7).

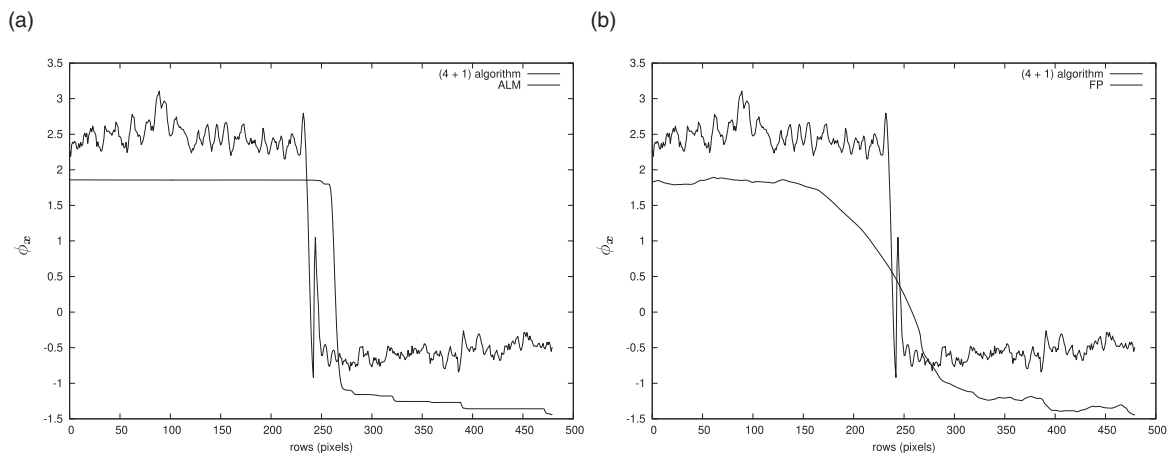


Figure 7. Middle column of the estimated phase terms using (a) augmented Lagrangian method, equation (16), and (b) fixed point method, equation (7).

Conclusions

In this article, we present a reformulation of the method presented in Legarda-Saenz et al.⁸ as a constrained minimization problem and we solve it using the ALM. As can be seen in the numerical experiments, the proposed method is able to accurately demodulate

a single fringe pattern with discontinuities. The numerical solution of equation (16) results in a simple algorithm, which is faster and preserves the dynamic range of the phase term ϕ_x . An extra advantage of the proposed method is its feasibility to be implemented on dedicated hardware to obtain real-time processing. This will be one aim of our future research.


Declaration of Conflicting Interests


The author(s) declared no potential conflicts of interest with respect to the research, authorship, and/or publication of this article.

Funding

The author(s) received no financial support for the research, authorship, and/or publication of this article.

ORCID iDs

Ricardo Legarda-Saenz  <https://orcid.org/0000-0003-4875-324X>

Carlos Brito-Loeza  <https://orcid.org/0000-0003-2970-2113>

References

- Servin M, Quiroga JA and Padilla M. *Fringe pattern analysis for optical metrology: theory, algorithms, and applications*. Weinheim: Wiley-VCH, 2014.
- Marroquin JL, Rivera M, Botello S, et al. Regularization methods for processing fringe-pattern images. *Appl Opt* 1999; 38: 788–794.
- Legarda-Sáenz R, Osten W and Jüptner W. Improvement of the regularized phase tracking technique for the processing of nonnormalized fringe patterns. *Appl Opt* 2002; 41: 5519–5526.
- Villa J, Quiroga JA and Servin M. Improved regularized phase-tracking technique for the processing of squared-grating deflectograms. *Appl Opt* 2000; 39: 502–508.
- Rivera M. Robust phase demodulation of interferograms with open or closed fringes. *J Opt Soc Am A* 2005; 22: 1170–1175.
- Galvan C and Rivera M. Second-order robust regularization cost function for detecting and reconstructing phase discontinuities. *Appl Opt* 2006; 45: 353–359.
- Rudin LI, Osher S and Fatemi E. Nonlinear total variation based noise removal algorithms. *Physica D* 1992; 60: 259–268.
- Legarda-Saenz R, Brito-Loeza C and Espinosa-Romero A. Total variation regularization cost function for demodulating phase discontinuities. *Appl Opt* 2014; 53: 2297–2301.
- Brito-Loeza C, Legarda-Saenz R and Martin-Gonzalez A. A fast algorithm for a total variation based phase demodulation model. *Numer Methods Partial Differ Equations* 2020; 36: 617–636. DOI: 10.1002/num.22444; <https://doi.org/10.1002/num.22444>
- Vogel CR and Oman ME. Iterative methods for total variation denoising. *SIAM J Sci Comput* 1996; 17: 227–238.
- Vogel CR. *Computational methods for inverse problems*. Philadelphia, PA: SIAM, 2002.
- Chan TF, Golub GH and Mulet P. A nonlinear primal-dual method for total variation-based image restoration. *SIAM J Sci Comput* 1999; 20: 1964–1977.
- Chambolle A. An algorithm for total variation minimization and applications. *J Math Imaging Vision* 2004; 20: 89–97.
- Getreuer P. Rudin–Osher–Fatemi total variation denoising using split Bregman. *Image Process On Line* 2012; 2: 74–20.
- Hestenes MR. Multiplier and gradient methods. *J Optim Theory Appl* 1969; 4: 303–320.
- Rockafellar RT. A dual approach to solving nonlinear programming problems by unconstrained optimization. *Math Programm* 1973; 5: 354–373.
- Bertsekas DP. *Constrained optimization and Lagrange multiplier methods*. Belmont, MA: Athena Scientific, 1996.
- Nocedal J and Wright S. *Numerical optimization*. 2nd ed. New York, NY: Springer, 2006.
- Tai XC and Wu C. Augmented Lagrangian method, dual methods and split Bregman iteration for ROF model. In: *Second international conference, SSVN*, Norway, 1–5 June, 2009, Vol. LNCS 5567, pp. 502–513. DOI: 10.1007/978-3-642-02256-2_42; http://dx.doi.org/10.1007/978-3-642-02256-2_{_}42
- Wu C and Tai XC. Augmented Lagrangian method, dual methods, and split Bregman iteration for ROF, vectorial TV, and high order models. *SIAM J Imaging Sci* 2010; 3: 300–339.
- Donoho D. De-noising by soft-thresholding. *IEEE Trans Inform Theory* 1995; 41: 613–627.
- Wang Y, Yang J, Yin W, et al. A new alternating minimization algorithm for total variation image reconstruction. *SIAM J Imaging Sci* 2008; 1: 248–272.
- Caboussat A, Glowinski R and Pons V. An augmented Lagrangian approach to the numerical solution of a non-smooth eigenvalue problem. *J Numer Math* 2009; 17: 3–26.
- Bertero M and Boccacci P. *Introduction to inverse problems in imaging*. Bristol: Institute of Physics Publishing, 1998.
- Perlin M and Bustamante MD. A robust quantitative comparison criterion of two signals based on the Sobolev norm of their difference. *J Eng Math* 2016; 101: 115–124.
- Kreis T. *Holographic interferometry: principles and methods*. Berlin: Wiley-VCH, 1996.